electronics

MDPI

Article

Investigation of a Miniaturized E-Band Cosine-Vane Folded Waveguide Traveling-Wave Tube for Wireless Communication

Kexin Ma, Jun Cai * and Jinjun Feng

National Key Laboratory of Science and Technology on Vacuum Electronics, Beijing Vacuum Electronics Research Institute, Beijing 100015, China; makexin@163.com (K.M.); fengjj@ieee.org (J.F.)
* Correspondence: caijun@sdu.edu.cn; Tel.: +86-130-2615-5686

Abstract: To realize the miniaturization of E-band traveling-wave tubes (TWTs), the size analysis and optimization design were carried out based on an improved cosine-vane folded waveguide (CV-FWG) slow-wave structure (SWS) that operates in a low voltage. In addition, a novel miniaturized T-shaped coupler was proposed to achieve a good voltage standing wave rate (VSWR) in a broad bandwidth. The coupler length was reduced by as much as 77% relative to an original design. With higher coupling impedance, the radius and length of the shortened SWS were optimized as 1.3 mm and 50 mm, respectively. Using microwave tube simulator suit (MTSS) and CST particle studio (PS), 3D beam–wave simulations at 9400 V, 20 mA predicted a gain of 20 dB and a saturated output power of 9 W. The simulation results for CV-FWG TWTs were compared with conventional FWG TWTs from 81 GHz to 86 GHz, showing significant performance advantages with excellent flatness for high-rate wireless communication in the future. The CV-FWG SWS circuit will be fabricated by 3D printing, and this work is underway.

Keywords: TWT; E-band; wireless communication; cosine-vane; FWG; miniaturization

Citation: Ma, K.; Cai, J.; Feng, J. Investigation of a Miniaturized E-Band Cosine-Vane Folded Waveguide Traveling-Wave Tube for Wireless Communication. *Electronics* **2021**, *10*, 3054. https://doi.org/10.3390/electronics10243054

Academic Editor: Alessandro Gabrielli

Received: 10 November 2021
Accepted: 5 December 2021
Published: 7 December 2021

1. Introduction

The Federal Communications Commission (FCC) opened up the E-band (71–76 GHz and 81–86 GHz) for millimeter wave frequency microwave communication [1]. It can meet the demands of high data rate communication with 10 GHz available bandwidth [2]. The transmission rate of E-band can reach 100 Gbit/s, which enables numerous applications, such as local area networks, broadband metropolitan links, back-haul interconnects, and transmissions among next-generation base stations [3–5]. Due to atmospheric and rain attenuation, a high-power amplifier is required to ensure the transmission distance and signal coverage area.

Among vacuum electron devices (VEDs), the traveling-wave tube (TWT) is a preferable choice for millimeter waves, which have high power and wide bandwidth [6–8]. There is much research on E-band TWTs. L-3 Electron Devices division (CA, USA) developed a CW E-band microwave power module (MPM) to cover 81–86 GHz for communication applications. The power amplifier in the MPM is a folded waveguide (FWG) TWT, capable of 80 W saturated output power at 20.8 kV, 220 mA [9]. BVERI developed an E-band TWT that can produce more than 75 W continuous wave saturated output power over the range of 81–86 GHz with a voltage of 16.3 kV and a current of 105 mA [10]. UESTC developed an E-band FWG TWT. The experimental results showed that the prototype tube covers the bandwidth of 83–86 GHz with an output power above 30 W. The tube is tested when the electron gun voltage is 17 kV and the beam current is 62 mA [11]. Both of these TWTs have a large structure size and work at high voltage and high current.

Moreover, the size of the devices is also crucial as TWTs are mounted on the compact platform with a limited space. A 94 GHz, 25 W compact helical TWT for operating at 9700 V, 13.5 mA is being developed with a size of 66.04 mm × 48.26 mm × 48.26 mm [12]. Utilizing the same design rules and fabrication technology, an E-band TWT with a saturated output

power of 8 W will be built [13]. Due to the high technical complexity, no subsequent test results have been published so far.

Compared to the helix slow-wave structure (SWS), folded waveguide (FWG) SWS is widely used in millimeter waves. Otherwise, the transverse size of the FWG determines the cutoff frequency of the waveguide, which is difficult to reduce to realize miniaturization. The cosine-vane FWG (CV-FWG) could achieve a significant decrease in the cutoff frequency, which facilitates a transverse miniaturized design of the SWS [14].

This paper is organized as follows. The introduction is presented in Section 1. Section 2 gives the effects of various structure parameters on the cold characteristics. The design of a miniaturized high-frequency structure is described in Section 3, which includes a miniaturized SWS, a miniaturized T-shaped coupler, and the simulation of a beam–wave interaction. Finally, a conclusion is drawn in Section 4.

2. Analysis of Cold Characteristics

Based on normal CV-FWG [14], a modified CV-FWG was studied to add design dimensions by changing the height of the waveguide-connecting section and name it as d as shown in Figure 1. The structural parameter d makes the structural design more flexible. Figure 1a shows the 3D cut-away of a CV-FWG SWS in a single period, where a is the width of the waveguide, b is the width of the narrow side, $2p$ is the geometric period, h is the height of the straight waveguide, r_c is the radius of the electron beam channel, and A_c is the amplitude of the cosine curve whose value could be chosen from zero (conventional FWG) to the sum of $h/2$ and $d/2$, and Figure 1b shows a cross-sectional view of the CV-FWG. CV-FWG can be regarded as the combination of FWG and a staggered double vane when the value of Ac is greater than $h/4$, the symmetrical profiling in x-axis of CV-FWG can be seen as a FWG, and the end view of the CV-FWG can be seen as a staggered double vane. With the increase of Ac, the proportion of staggered double vane increases gradually.

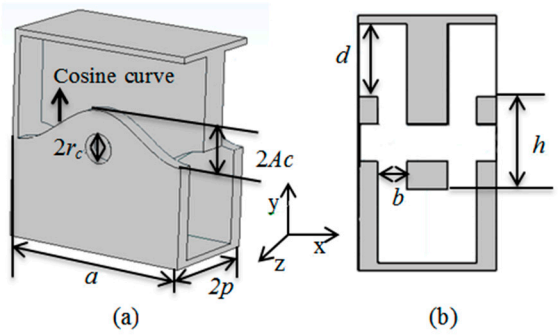

Figure 1. Schematic of single period CV-FWG: (**a**) 3D cut-away solid model and (**b**) cross-sectional view of the CV-FWG.

To realize the miniaturization of SWS, the influences of structure parameters on cold characteristics were analyzed. For the CV-FWG, only the Ac and d need to be illustrated, the influences of the other structure parameters, including a, b, p, and h, are similar to the conventional FWG.

As shown in Figure 2, the normalized phase velocity of CV-FWG decreases with the increase of Ac, and the cold bandwidth becomes wider; meanwhile, the cutoff frequency decreases rapidly. When the Ac is equal to 0, the SWS is a conventional FWG, and the dispersion is a normal dispersion. As the Ac increases, it becomes an abnormal dispersion. Figure 3 shows the effect of d on the dispersion. As d increases, the dispersion curves become flatter with the reduced intrinsic bandwidths. The normalized phase velocity in the frequency range below 55 GHz increases with the increase of d, while the trend reverses above 55 GHz. The cutoff frequency is almost constant.

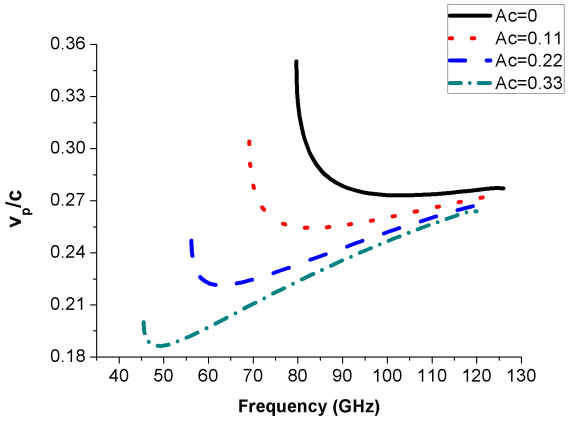

Figure 2. Normalized phase velocity of the CV-FWG for various values of *Ac*.

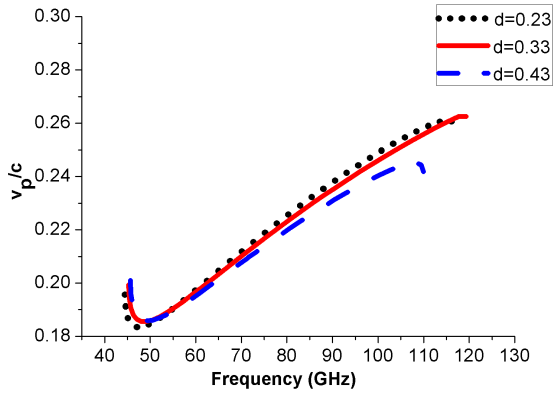

Figure 3. Normalized phase velocity of the CV-FWG for various values of *d*.

Figures 4 and 5 show the effects of the variations of *Ac* and *d* on the on-axis coupling impedance, respectively. At the operation frequency from 81–86 GHz, the on-axis coupling impedance is decreased with the increase of *Ac*, and the curve is flatter, while it is increased with the increase of *d*, and the on-axis coupling impedance flatness are similar to each other.

The loss was calculated with the conductivity of 1.6×10^7 S/m. As shown in Figure 6, with the increase of the *Ac*, the loss is decreased. But the effect of the *d* on the loss is complex as shown in Figure 7. In the frequency range from 81–86 GHz, the variation of loss is within 0.3 dB/m. Though the change is not obvious, when *d* and *h* are adjusted simultaneously, the loss decreases and the coupling impedance increases, while the dispersion is almost unchanged, which is important for the optimized design in the next section.

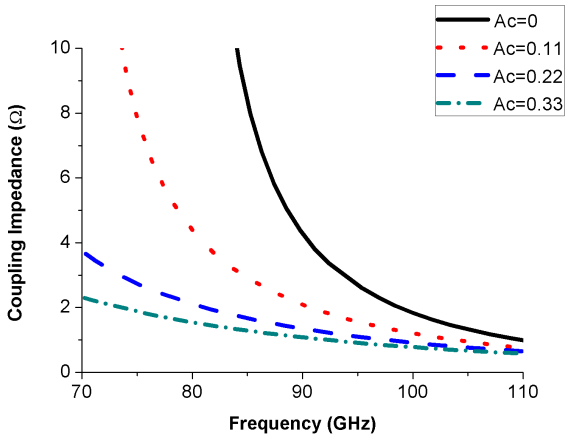

Figure 4. Coupling impedance of the CV-FWG for various values of *Ac*.

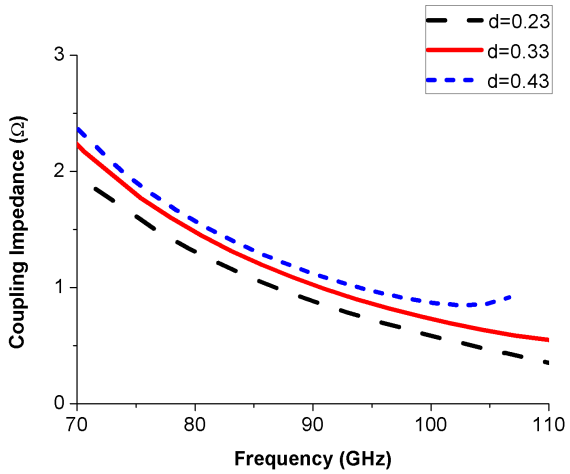

Figure 5. Coupling impedance of the CV-FWG for various values of *d*.

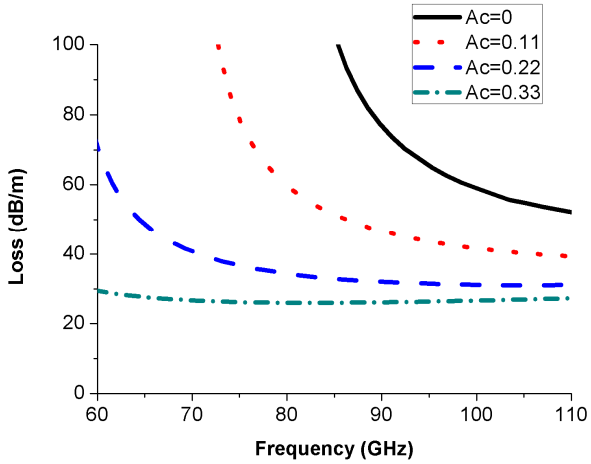

Figure 6. Loss of the CV-FWG for various values of *Ac*.

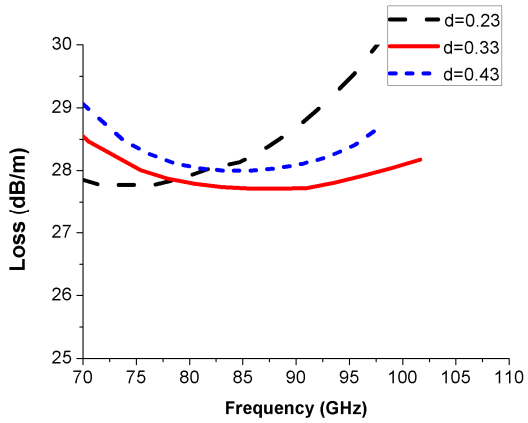

Figure 7. Loss of the CV-FWG for various values of *d*.

3. Design of Device

3.1. Design of SWS

Based on the above analysis, the operational parameters are shown in Table 1. Several SWS designs were investigated to minimize size and make the SWS operate at the designated voltage. The final structure parameters are shown in Table 2. To show the advantages of CV-FWG, a FWG with a similar dispersion in the operation frequency band

was designed for comparison, and the structure parameters are also shown in Table 2. Two cross-section structures are compared in Figure 8. The R_1 and R_2 are the radii of the FWG and CV-FWG, respectively. Compared to the FWG, the radius of CV-FWG is reduced by 23.5%, and the area of the cross-section is reduced by 41.8%.

Table 1. Operational parameters.

Frequency	**81–86 GHz**
Beam voltage	Less than 10 kV
Beam current	Less than 20 mA
Peak output power	More than 8 W
RF input/output	WR-10

Table 2. Structure parameters and comparison.

Parameter	**Dimensions (mm)**		**Reduction Percentage (%)**
	CV-FWG	**FWG**	
a	1.6	2.4	33
b	0.2	0.3	33.33
p	0.45	0.55	18
h	0.6	1	40
r_c	0.12	0.12	0
Ac	0.2	-	-
d	0.5	-	-
R	1.3	1.7	23.5
S (mm^2)	5.3	9.1	41.8

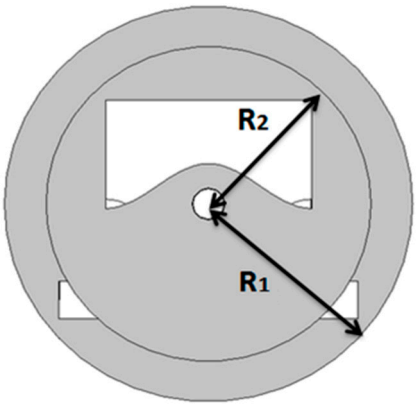

Figure 8. Cross-sectional view of CV-FWG and FWG.

The dispersion curves of CV-FWG and FWG are shown in Figure 9. The dispersions of the two structures are almost identical in the operation frequency from 81–86 GHz, and the curve is very flat with the variation of 0.00025. The loss and the on-axis coupling impedance are compared as shown in Figures 10 and 11. The on-axis coupling impedances for CV-FWG and FWG are 6.5 Ω and 2.1 Ω, respectively; at 81 GHz, the coupling impedance of the CV-FWG is about three times higher than that of the FWG. And at 86 GHz, the coupling impedances are 4.4 Ω and 1.4 Ω, respectively. The coupling impedance of CV-FWG is about 3.2 times higher than that of FWG. Figure 11 shows the losses of the CV-FWG and FWG. Compared with FWG, the loss of CV-FWG is increased by 31.6% at 81 GHz and 35.6% at 86 GHz. It can be seen that, compared with the FWG, the increase of the coupling impedance of CV-FWG is much larger than the increase of the loss. As a result, an increased interaction can be expected.

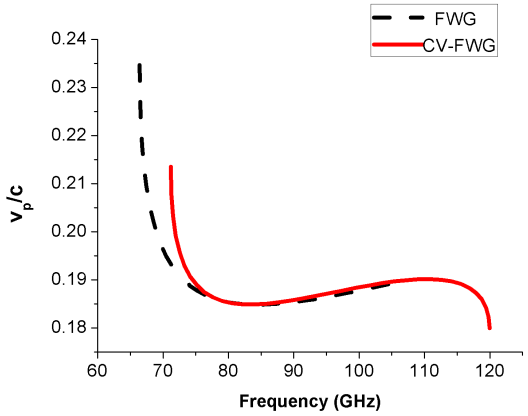

Figure 9. Normalized phase velocity of CV-FWG and conventional FWG.

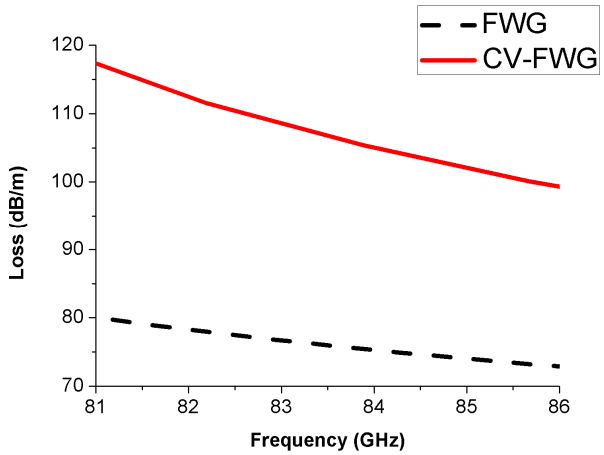

Figure 10. Transmission loss of CV-FWG and conventional FWG.

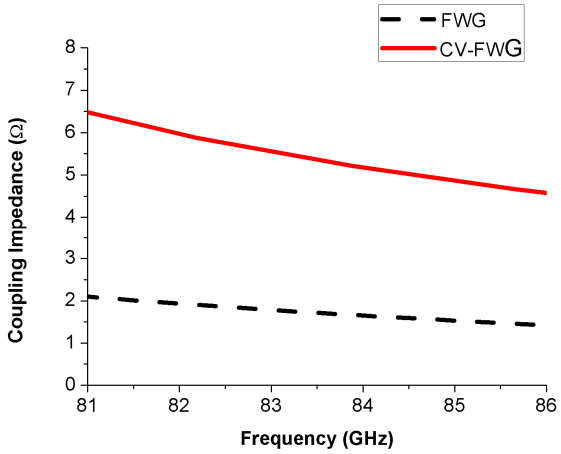

Figure 11. Coupling impedance of CV-FWG and conventional FWG.

It should be pointed out that the on-axis coupling impedance and loss for CV-FWG are smaller than those for FWG in [11], which is different from the above simulation results. The reason is that the comparison is carried out under the same structure parameters in [11]. To obtain consistency and good cold characteristics in the operation frequency band, the operation point of CV-FWG moves to the left, which leads to the increases of loss and on-axis coupling impedance, and the effect of on-axis coupling impedance is more apparent.

3.2. Miniaturized Coupler

It is impossible for CV-FWG to be directly coupled by a WR-10 standard rectangular waveguide. For miniaturization of the tube, a novel coupler named a T-shaped coupler was proposed, as shown in Figure 12.

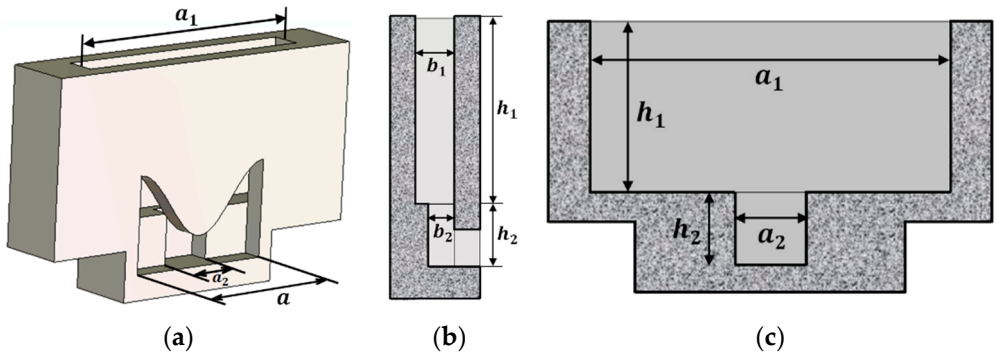

Figure 12. Schematic of the T-coupler: (**a**) 3D cut-away solid model, (**b**) front view of the T-coupler, and (**c**) cross-sectional view of the T-coupler.

The coupler can be regarded as the superposition of two rectangular waveguides with different sizes of length, width, and height. The a_1 and a_2 are the length of the upper rectangular waveguide and the lower rectangular waveguide, respectively. The b_1 and b_2 are the width of the upper rectangular waveguide and the lower rectangular waveguide, respectively. The h_1 and h_2 are the height of the upper rectangular waveguide and the lower rectangular waveguide, respectively.

Using CST Microwave Studio (MWS), the T-shaped coupler was optimized to meet the requirements of the E-band CV-FWG. Considering the difficulty in machining and the roughness of the circuit wall, the conductivity was set to 1.6×10^7 S/m. Figure 13 shows the voltage standing wave ratio (VSWR) as a function of frequency. The VSWR is $\leq$1.25 from 80 GHz to 90 GHz. The miniaturized design was realized because b_1 is equal to 0.3 mm, which is much smaller than the width of a WR-10 standard rectangular waveguide. The coupler length is reduced by as much as 77% relative to an original design.

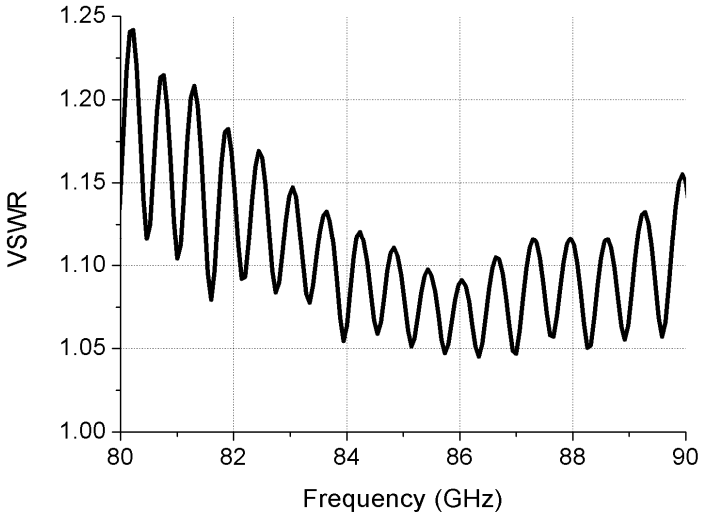

Figure 13. Matching characteristics of the T-shaped coupler.

3.3. Beam–Wave Interaction

The beam–wave interaction circuit was firstly carried out and optimized by microwave tube simulator suit (MTSS) software, then the result was verified by CST Particle Studio

(PS). Figure 14 shows the results of the saturated output power, and the gain for the CV-FWG and FWG were calculated by MTSS with the same operation voltage, current, and interaction length. The saturated output power of CV-FWG is greater than 8 W and the gain is greater than 19 dB, while output power of FWG is less than 2 W and the gain is less than 13 dB. It was proved that the beam–wave interaction of CV-FWG is stronger compared to the FWG and facilitates the reduction of the length of SWS.

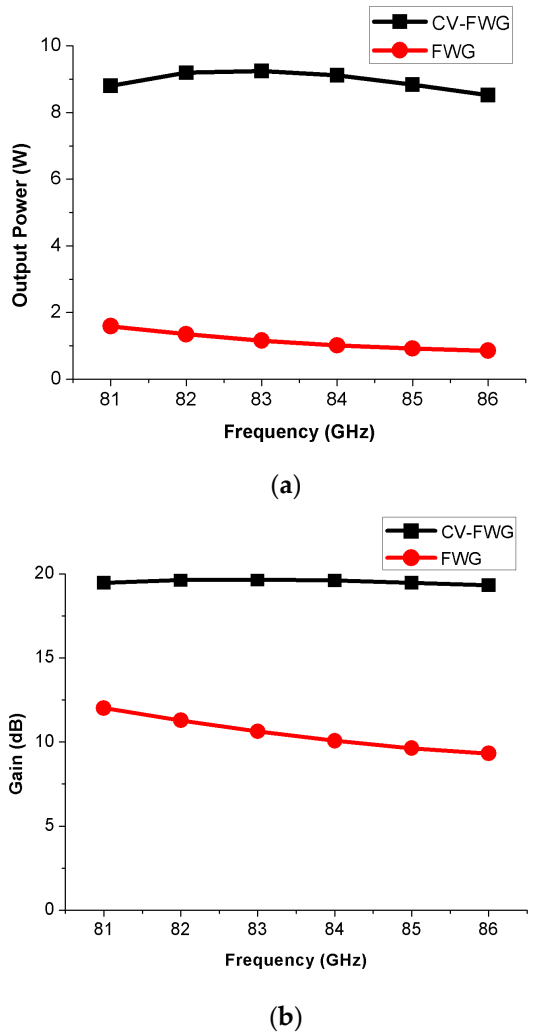

Figure 14. The output power (**a**) and gain (**b**) of CV-FWG and FWG simulated by MTSS.

3D PIC simulation software was used to predict the whole tube performance. A 3D model of a single section CV-FWG was built, which included the input and output couplers and a lossy metal housing (the conductivity was 1.6×10^7 S/m as shown in Figure 15. The PIC simulations were carried out on a cloud computing platform with about seven million mesh cells. Then the beam–wave interaction was calculated with a voltage of 9400 V, a current of 20 mA, and an interaction length of less than 50 mm. The radius of the electron beam is 0.06 mm, which is half of the radius of the electron beam channel. A sinusoidal RF-driven signal was applied. A uniform longitudinal magnetic field of 0.28 T was used in the PIC simulation. The simulation time is 6 ns for the bunching and amplifying. The total number of particles in the model is related to the model size and the simulation time. There are more than 1.73 million particles in this model. Figure 16 shows an amplified output signal at 83 GHz, with saturated power of more than 10 W less than 90 mW. The results of saturated power and gain are shown in Figure 17.

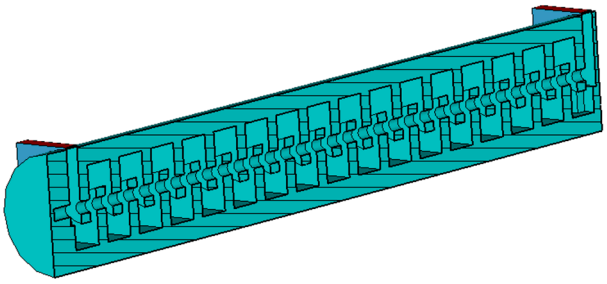

Figure 15. Cross-sectional view of SWS with T-coupler.

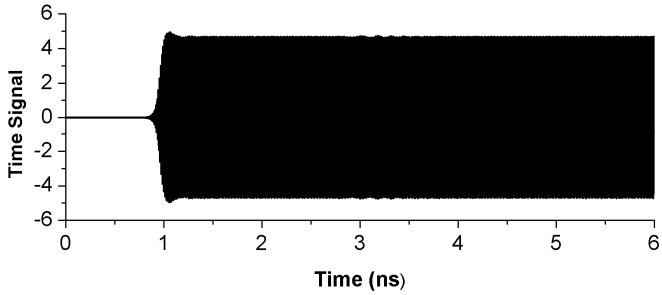

Figure 16. The output signal with 90 mW driven power.

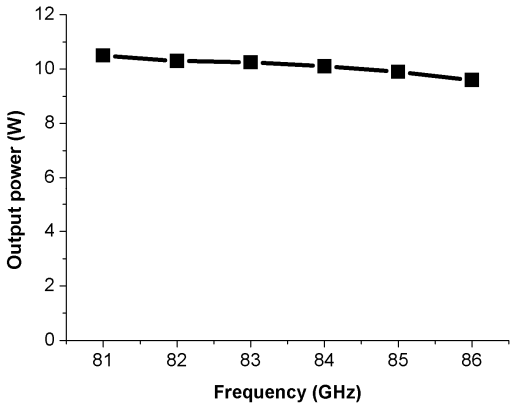

(**a**)

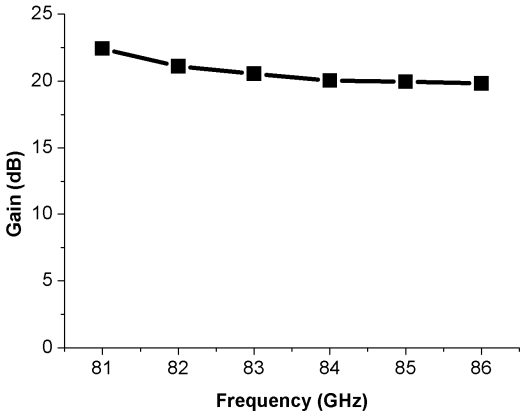

(**b**)

Figure 17. The output power (**a**) and gain (**b**) of CV-FWG simulated by PIC.

It can be seen that the saturated output power of CV-FWG is more than 9 W, and the saturated output power is 10.83 W in 83 GHz. The gain of the CV-FWG is about 20 dB. The gain varies within 20 dB from 81 GHz to 86 GHz. It shows that the gain has great consistency, which means the gain varies very little with frequency. Because the gain is more than 20 dB, the circuit was designed with 0 mW driven and the result indicated the single section slow-wave circuit will not oscillate and the performance of CV-FWG is steady.

4. Conclusions

We introduced a miniaturized CV-FWG SWS that was designed to operate in the voltage <10 kV from 81 GHz to 86 GHz. The dimensions of the CV-FWG SWS are 1.6 mm × 1.6 mm × 47.75 mm. To couple the CV-FWG, a compact T-shaped coupler was proposed with a good matching property. Lastly, the beam–wave interaction was simulated, and the saturated output power is more than 9 W, and the gain has great consistency. This research laid a foundation for the development of follow-up devices, which can be widely used in high data rate wireless communication.

Author Contributions: Conceptualization, K.M. and J.C.; methodology, K.M.; validation, J.C.; formal analysis, K.M.; writing-original draft preparation, K.M.; writing-review and editing, J.F. and J.C.; visualization, K.M.; funding acquisition, J.F. and J.C.; All authors have read and agreed to the published version of the manuscript.

Funding: This research was funded by National Natural Science Foundation of China grant number 61831001.

Conflicts of Interest: The authors declare no conflict of interest.

References

1. Federal Communication Commission: FCC 03-248. *Allocation and Service Rules for the 71-76GHz, 81-86GHz, and 92-95GHz Bands*; Federal Communications Commission: Washington, DC, USA, 2003.
2. Lu, J.; Zhou, Z.; Wang, L.; Zeng, J.; Chen, S. Zero-multiplication TX-filter structure for E-band Transmission system. In Proceedings of the 2014 International Conference on Information and Communications Technologies, Nanjing, China, 16–18 May 2014; pp. 1–5.
3. Ferndahl, M.; Gavell, M.; Abbasi, M.; Zirath, H. Highly integrated E-band direct conversion receiver. In Proceedings of the 2012 IEEE Compound Semiconductor Integrated Circuit Symposium, La Jolla, CA, USA, 14–17 October 2012; pp. 1–4.
4. Ghassemi, N.; Wu, K. Planar High-Gain Dielectric-Loaded Antipodal Linearly Tapered Slot Antenna for E- and W-Band Gigabyte Point-to-Point Wireless Services. *IEEE Trans. Antennas Propag.* **2013**, *61*, 1747–1755. [CrossRef]
5. Ghassemi, N.; Gauthier, J.; Wu, K. Low-Cost E-Band Receiver Front-End Development for Gigabyte Point-to-Point Wireless Communications. In Proceedings of the 43rd European Microwave Conference, Nuremberg, Germany, 6–10 October 2013; pp. 1011–1014.
6. Pan, P.; Zi, Z.; Cai, J.; Tang, Y.; Liu, S.; Xie, Q.; Bian, X.; Feng, J. Millimeter Wave Traveling Tubes for High Data Rate Wireless Communication. *Acta Electronica Sinica* **2020**, *48*, 1834–1840.
7. Li, Y.; Yue, L.; Qiu, B.; Gao, H.; Wang, S.; Zhao, G.; Xu, J.; Yin, H.; Duan, Z.; Huang, M.; et al. Design and Cold Test of a Ka-band Fan-Shaped Metal Loaded Helix Traveling Wave Tube. In Proceedings of the 2020 IEEE 21st International Conference on Vacuum Electronics (IVEC), Monterey, CA, USA, 19–22 October 2020; pp. 241–242.
8. Liu, S.; Xie, Q.; Chen, Z.; Wu, Y.; Zi, Z.; Wu, X.; Cai, J.; Feng, J. High Linear Power E-Band Traveling-Wave Tube for Communication Applications. *IEEE Trans. Electron Devices* **2021**, *68*, 2984–2989. [CrossRef]
9. Kowalczyk, D.; Zubyk, A.; Meadows, C.; Schoemehl, T.; True, T.; Martin, M.; Kirshner, M.; Armstrong, C. High Efficiency E-Band MPM for Communications Applications. In Proceedings of the IEEE 17th International Vacuum Electronics Conference (IVEC), Monterey, CA, USA, 19–21 April 2016; pp. 513–514.
10. Zi, Z.; Liu, S.; Xie, Q.; Li, S.; Cai, J.; Zhao, S. A 70W 81-86GHz E-band CW Traveling Tube. In Proceedings of the IEEE International Vacuum Electronics, Busan, Korea, 28 April–1 May 2019; pp. 1–2.
11. Ji, R.; Yang, Z.; Guo, Z.; Wang, Q.; Han, P.; Gong, H. Design and Experiment of An E-band Folded Waveguide Traveling Wave Tube. In Proceedings of the IEEE 20th International Vacuum Electronics Conference (IVEC), Busan, Korea, 28 April–1 May 2019; pp. 1–2.
12. Kory, C.; Dayton, J.; Mearini, G.; Lueck, M. Microfabricated 94 GHz TWT. In Proceedings of the International Vacuum Electronics, Monterey, CA, USA, 17 July 2014; pp. 175–176.
13. Dayton, J.; Kory, C.; Mearini, G. Microfabricated mm-wave TWT Platform for Wireless Backhaul. In Proceedings of the International Vacuum Electronics, Beijing, China, 27 August 2015; pp. 1–2.
14. Cai, J.; Wu, X.; Feng, J. A Cosine-Shaped Vane-Folded Waveguide and Ridge Waveguide Coupler. *IEEE Trans. Electron Devices* **2016**, *63*, 2544–2549. [CrossRef]